JOURNAL OF GEOPHYSICAL RESEARCH, VOL. 113, D12207, doi:10.1029/2007JD009371, 2008

Open cellular structure in marine stratocumulus sheets

R. Wood,[1] K. K. Comstock,[1] C. S. Bretherton,[1] C. Cornish,[1] J. Tomlinson,[2,3] D. R. Collins,[2] and C. Fairall[4]

Received 10 September 2007; revised 8 January 2008; accepted 2 April 2008; published 25 June 2008.

[1] Geostationary and Sun-synchronous satellite data and in situ observations from ship cruises are used to investigate the formation of open cellular structure in marine stratocumulus clouds over the southeast Pacific (SEP). Open cellular convection either forms spontaneously as pockets of open cells (POCs) within overcast stratocumulus, or is advected into the region from midlatitude regions. POC formation occurs most frequently during the latter part of the night, demonstrating that this transition is not caused by solar absorption-driven decoupling. The transition preferentially occurs in clouds with low 11–3.9 μm nighttime brightness temperature difference (BTD) which is found to be well correlated with both in situ measured accumulation mode aerosol concentration and cloud droplet concentration estimates derived from MODIS. Besides indicating that nighttime BTD is an excellent proxy for stratocumulus cloud droplet concentration N_d, this also suggests that low aerosol concentrations favor POC formation. Indeed, extremely low accumulation mode aerosol concentrations are found during the passage of open cell events over the ship. Free-tropospheric moisture is not found to be an important factor in POC formation. Significant subseasonal variability occurs in the fractional coverage of open cellular convection over the broader SEP. This coverage is well correlated with a MODIS-derived drizzle proxy (MDP) proportional to the ratio of liquid water path (LWP) to N_d for predominantly overcast regions. Both LWP and N_d variability influences the MDP. Periods of low MDP have significant positive large-scale N_d anomalies and are preceded by offshore winds at 850 hPa, which suggests a potential continental influence upon open cell formation over the SEP. Together, the results suggest important two-way interactions between aerosols and drizzle in marine stratocumulus and a role for drizzle in modulating the large-scale albedo of these cloud systems.

Citation: Wood, R., K. K. Comstock, C. S. Bretherton, C. Cornish, J. Tomlinson, D. R. Collins, and C. Fairall (2008), Open cellular structure in marine stratocumulus sheets, *J. Geophys. Res.*, *113*, D12207, doi:10.1029/2007JD009371.

1. Introduction

[2] Marine boundary layer (MBL) cloud cover over the eastern subtropical oceans is strongly dependent upon the dominant form of mesoscale cellular convection (MCC) that is present [*Agee et al.*, 1973; *Wood and Hartmann*, 2006]. Over the cooler regions, especially in the southeast Pacific (SEP), two forms of MCC dominate: closed MCC with extensive cloud cover and open MCC with much lower cloud cover. Cloud cover in critical for determining albedo and so it is important to understand the processes controlling the relative amounts of closed and open MCC. Although open MCC tends to be more commonly located downstream of closed MCC, at any particular location there is a lack of sensitivity of the MCC type upon large-scale meteorological conditions [*Wood and Hartmann*, 2006]. It is therefore possible that a mechanism internal to the MBL may be important in determining the transition from closed to open MCC.

[3] There is a paucity of in situ data on MCC transitions. *Stevens et al.* [2005], using case studies from recent field campaigns, finds that broad regions of open MCC and pockets of open cells (POCs) within overcast stratocumulus have similar characteristics, specifically strong drizzle and longevity. Strong drizzle seems to be a common feature of open MCC [*Comstock et al.*, 2005, 2007; *Sharon et al.*, 2006]. Low values of the 11–3.9 μm brightness temperature difference (BTD) have been observed in and around POCs [*Stevens et al.*, 2005; *Van Zanten et al.*, 2005] indicating large cloud droplets [*Pérez et al.*, 2000]. Very low accumulation mode aerosol concentrations have been observed in POCs [*Petters et al.*, 2006; *Sharon et al.*, 2006]. To what extent are these limited studies of the connections between the microphysical and the macrophysical properties of POCs representative of behavior over the broader subtropical eastern oceans? And does microphysical variability in overcast stratocumulus influence the susceptibility of these

[1]Department of Atmospheric Sciences, University of Washington, Seattle, Washington, USA.
[2]Department of Atmospheric Sciences, Texas A&M University, College Station, Texas, USA.
[3]Now at Pacific Northwest National Laboratory, Richland, Washington, USA.
[4]Earth System Research Laboratory, NOAA, Boulder, Colorado, USA.

0148-0227/08/2007JD009371$09.00

clouds to the transition from closed to open MCC, or are the distinct microphysics of open cellular regions merely a response to other factors driving the transition?

[4] In this study characteristics of open cellular clouds over the SEP are examined in an attempt to understand in a more general sense the characteristics and formation of these systems. We use a combination of geostationary and Sun-synchronous satellite data, in situ data, and back trajectory analysis. Section 2 describes the data sets we use, while section 3 contains an assessment of the derived satellite microphysical estimates used in this study. In section 4 we present two case studies of open cellular convection. Section 5 describes a more statistical approach to understanding the properties of open cellular convection, and section 6 describes the associated meteorological variability. Sections 7 and 8 provide a brief discussion and conclusions.

2. Data

2.1. Satellite Data

[5] Satellite data from the NOAA Geostationary Operational Environment Satellite (GOES) [*Menzel and Purdom*, 1994] and from the Moderate Resolution Imaging Spectroradiometer (MODIS) [*King et al.*, 1992] are used in this study.

2.1.1. GOES Data

[6] We use GOES 8 whole disk scans, which are available approximately every 3 h. For 2001 we use data from September and October to develop a map to compare with daytime visible/near-infrared MODIS cloud retrievals (see section 3.1). For 2003 and 2004 we use data at all times of day for the period of the ship cruises detailed below. We use visible (VIS, channel 1, 0.55–0.75 μm), thermal infrared (TIR, channel 4, 10.2–11.2 μm) and near infrared (NIR, channel 2, 3.84–4.06 μm) channels from GOES. The TIR and NIR radiances are provided as brightness temperature (T_b). All satellite data are first interpolated to 5 km resolution. The brightness temperature difference $T_b^{TIR} - T_b^{NIR}$, when derived from nighttime data, is referred to as BTD throughout this study. We describe derived products from the GOES radiances in section 3.

[7] We derive the mean nighttime BTD for all cloudy pixels from September/October 2001 in the region 5–30°S, 70–100°W. This preliminary attempt at a BTD climatology is compared against quantitative microphysical retrievals from MODIS (section 3.1). To screen for the presence of clouds we use a thresholding technique based upon the September/October mean sea surface temperature *SST* from the Advanced Microwave Scanning Radiometer [*Wentz and Meissner*, 2000] (additional information regarding these products is available online at http://www.remss.com). A GOES pixel is classified as cloudy if $SST\text{-}T_b^{TIR} > 5$ K, which is a somewhat more stringent criterion than is used in the International Satellite Cloud Climatology Project [*Rossow and Garder*, 1993], designed to reduce the contamination from broken clouds. The particular choice of threshold does have some impact upon the mean BTD values obtained but the general behavior is unchanged.

[8] We use GOES data from individual scans to develop case studies of open cell formation and evolution, and to determine some statistics concerning the frequency of open cells from September/October 2001. Generally, GOES scans were made every 3 h (0245, 0545, 0845 UTC etc.) with some additional scans (typically these were between 0745–0945 UTC) on a number of days throughout the period. In addition, we use GOES data from individual scans colocated with the location of a research vessel (see below), comparing in situ aerosol measurements with satellite-derived estimates of microphysical properties in the MBL. This comparison is described in more detail in section 3.1.

2.1.2. MODIS Data

[9] MODIS standard cloud retrievals of cloud optical thickness τ and cloud top effective radius r_e [*King et al.*, 2003] are used to derive an estimate of the cloud droplet concentration N_d for warm clouds following *Szczodrak et al.* [2001], which assumes an adiabatic cloud layer with a constant droplet concentration. MODIS cloud top temperature and pressure estimates [*Menzel and Strabela*, 1997] provide the necessary thermodynamic parameters to convert from τ and r_e to N_d. The results are not strongly sensitive to precise specification of the temperature and pressure. N_d is most strongly influenced by variations in r_e rather than τ [*Szczodrak et al.*, 2001]. Global assessment of N_d from MODIS have been reported by *Bennartz* [2007]. The MODIS data are also used to derive an estimate of the cloud liquid water path (LWP), following *Wood and Hartmann* [2006], and these compare well with microwave-derived estimates [*Wood et al.*, 2002; *Bennartz*, 2007]. In this study we use the MODIS L3 daily $1° \times 1°$ gridded data product to derive a two month (September-October 2001) map of the mean N_d. To reduce contamination from broken clouds, which degrade cloud microphysical retrievals [*Coakley et al.*, 2005], we only include each daily value in the mean if its cloud cover exceeds 80%.

[10] MODIS is also used to provide nighttime BTD estimates for comparison with the in situ measurements. The thermal and near-infrared MODIS channels used are Ch31 (10.78–11.28 μm) and Ch20 (3.66–3.84 μm), which are close to those from GOES.

2.2. Cruise Data

[11] Data from three recent research vessel cruises during 2001, 2003 and 2004 are used in this study. The observations were made as part of the 2001 East Pacific Investigation of Climate field program (EPIC [see *Bretherton et al.*, 2004]) and the NOAA Pan American Climate Studies program (PACS) (further information on the cruises is available at http://www.etl.noaa.gov/programs/pacs/). The cruises took place during October 2001, November 2003 and December 2004, during the season of maximum stratus amount over the SEP [*Klein and Hartmann*, 1993]. All three cruises revealed a sharply defined marine boundary layer (MBL) with a strong capping inversion, extensive stratocumulus cloud cover, and frequent drizzle. Further analysis of the 2003 cruise is given by *Kollias et al.* [2004]. Table 1 and Figure 1 give more details on the 2003 and 2004 cruise data and tracks. Only data taken at 20°S, 85°W are used from the 2001 cruise, so we do not show the complete cruise track.

[12] On the 2003/2004 cruises a suite of aerosol measurements was made by the Texas A&M group [*Tomlinson et al.*, 2007]. In this paper we focus only upon the size distribution measured using a Differential Mobility Analy-

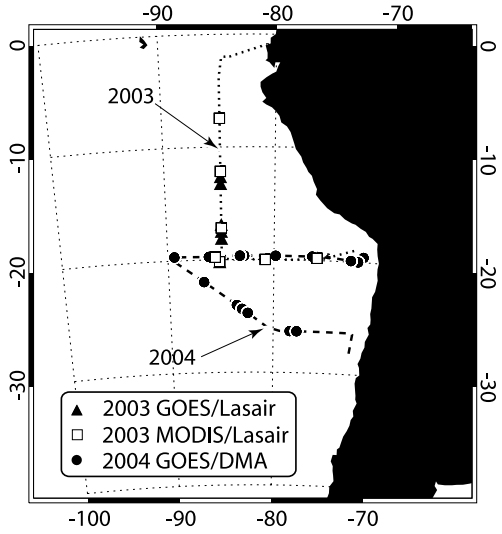

Figure 1. Tracks of 2003 and 2004 cruises and locations of satellite overpass comparisons. Symbols are as in Figure 3.

ser (DMA). The aerosol size distribution was strongly bimodal throughout most of the cruise with a sharp minimum separating an Aitken mode with a mean dry diameter of ~0.05 μm and an accumulation mode with a mean dry diameter of ~0.2 μm [*Tomlinson et al.*, 2007]. The minimum indicates aqueous phase oxidation of sulfur species to form sulfate [*Hoppel et al.*, 1986]. This is supported by volatility and hygroscopicity measurements on the cruise [*Tomlinson et al.*, 2007] indicating an aerosol composition rich in sulfate with little insoluble mass. We return to this point when discussing comparisons with satellite microphysical estimates in section 3.1. The accumulation mode concentration N_a from the DMA is defined as the concentration in the larger of the two modes, and so is effectively the concentration of particles with dry diameters 0.08–1.0 μm.

[13] For the 2003 cruise the accumulation mode aerosol concentration N_a was also estimated by summing the concentrations from all six diameter categories from 0.1 to 1.0 μm using a Particle Measuring Systems Lasair-II (http://www.pmeasuring.com) optical particle counter. Unlike the DMA, the Lasair does not dry the particles before sizing. At a relative humidity *RH* of 75% (a typical value for the cruises), hygroscopic growth factors for sulfate rich species are in the 1.3–1.4 range [*Tang and Munkelwitz*, 1994]. Thus, the dry diameter detection limit is likely somewhat less than 0.1 μm for the smallest Lasair size category but this may be offset by the use of polystyrene latex (which has a somewhat higher refractive index than water) to determine the diameter categories.

[14] Side by side comparison of the DMA and Lasair N_a reveals that the rms difference between the two N_a estimates is 30 cm^{-3} (or approximately 17%), with almost no mean bias. The reason for using the Lasair in 2003 is that this device functioned more or less continually during the 2003 cruise whereas there were more periods of outage for the DMA. In any case, the values of N_a are likely to be accurate to approximately 20% during both cruises. As we shall see, this uncertainty is relatively small compared with the range of variability encountered during the cruises.

[15] For the 2001 and 2003 cruises we also use millimeter radar and lidar ceilometer measurements to document cloud and precipitation changes for two case studies focusing upon open and closed cellular convection (section 4).

2.3. Reanalyses and Other Data Sets

[16] Daily mean reanalysis data from NCEP/NCAR [*Kistler et al.*, 2001] are used to (1) derive three-dimensional back trajectories for two case studies presented in this study and (2) examine the patterns of variability associated with open and closed cells. Reanalysis data are available on a 2.5 × 2.5° grid. We first interpolate these data onto the same 1° × 1° grid of the MODIS L3 data. In addition, 6 hourly water vapor fields from the European Centre for Medium-Range Weather Forecasts (ECMWF) reanalysis (ERA-40 [*Uppala et al.*, 2005]) are used to determine the free-tropospheric moisture during times of POC formation during 2001.

[17] We also use daily mean surface wind vector data from the SeaWinds 13.4 GHz microwave scatterometer on the NASA Quikbird satellite. We use the products generated by Remote Sensing Systems using the algorithm of *Wentz and Smith* [1999].

3. Derived Satellite Products

3.1. Satellite Microphysical Estimates

[18] In this section we assess the extent to which GOES nighttime BTD can give credible information about the cloud and aerosol microphysical properties in and under overcast stratocumulus. As pointed out by *Van Zanten and Stevens* [2005] BTD values for a scene containing broken clouds may not be indicative of microphysical properties but instead reflect cloud inhomogeneity because the BTD of the surface is typically close to zero, whereas we will see that the BTD for unbroken clouds is typically 1–4 K. We are therefore careful to screen our observations to remove noncloudy or partly cloudy pixels before aggregating to find mean values.

[19] We have two approaches. First, we compare the two month mean nighttime cloud-only GOES BTD map described above with the mean map of daytime MODIS estimated cloud droplet concentration for mostly cloudy

Table 1. Details of the Cruise Data Used in This Study

Cruise	2001	2003	2004
Vessel	R/V *Ronald H. Brown*	R/V *Roger Revelle*	R/V *Ronald H. Brown*
Dates[a]	10–24 Oct	14–24 Nov	6–21 Dec
Aerosol instruments	N/A	Lasair (size distribution 0.1–1.0 μm)	DMA (size distribution 0.01–0.75 μm)
Cruise reference	*Bretherton et al.* [2004]	*Kollias et al.* [2004]	http://www.etl.noaa.gov/programs/pacs/
Aerosol reference	N/A	*Tomlinson et al.* [2007]	*Tomlinson et al.* [2007]

[a]Dates given correspond to the periods of data used in this study, not necessarily the entire cruise.

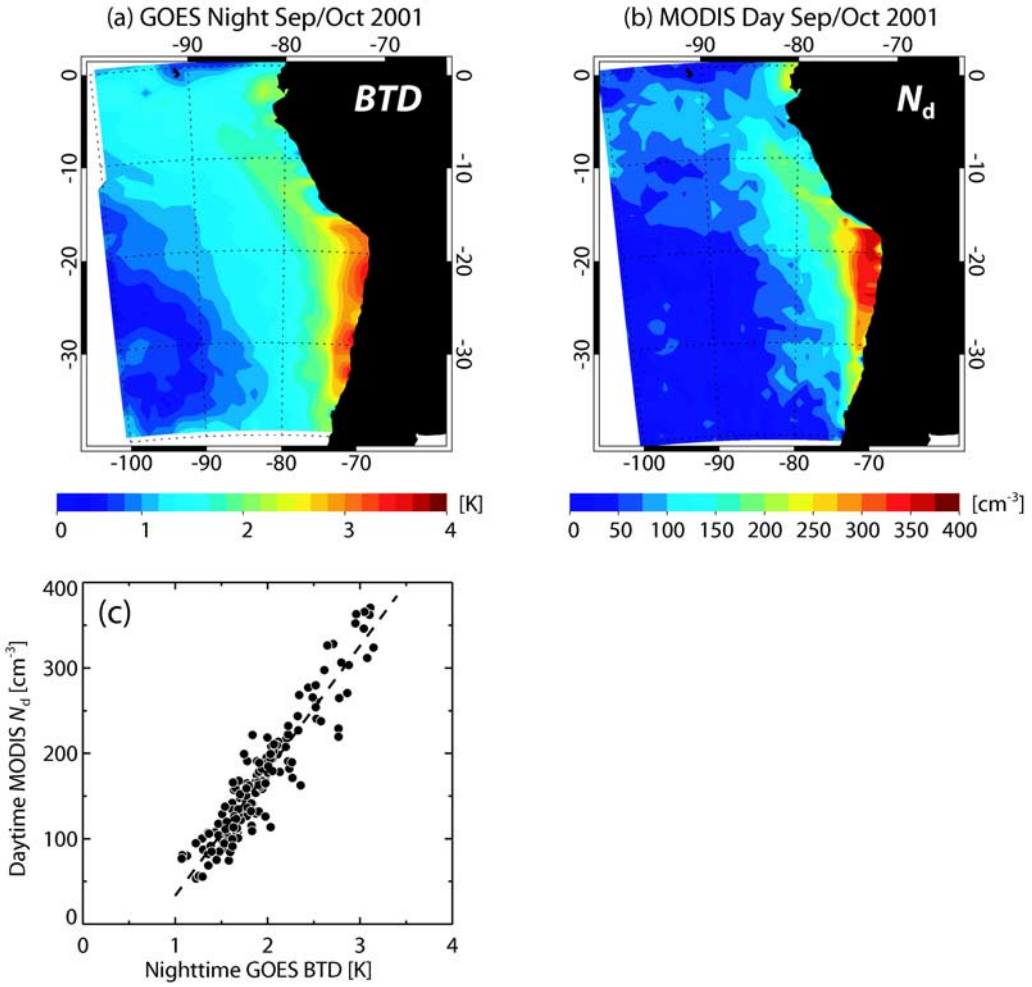

Figure 2. (a) Mean BTD from nighttime GOES data over all cloudy and low-variance pixels for September/October 2001 for 1° × 1° boxes. (b) Mean daytime cloud droplet concentration N_d for same period estimated from all Terra MODIS retrievals where cloud fraction exceeds 0.8 within 1° × 1° boxes. (c) Mean values of BTD and N_d data in Figures 2a and 2b for 1° × 1° regions for regions where at least one quarter of all available MODIS L2 data had cloud cover exceeding 0.8. This reduces the statistical sampling errors for regions with only a few acceptable MODIS retrievals. The dashed line is a linear fit to the data.

scenes. Comparing mean fields allows us to compare nighttime and daytime estimates without the need to worry about advection. Figure 2 shows these maps, together with a scatterplot of the 1 × 1° means demonstrating the remarkable degree of correlation between the two (r = 0.94), and indicating that nighttime BTD in overcast cases is an excellent proxy for the cloud droplet concentration N_d. That the MODIS data are from the day and the GOES from the night is unlikely to be a confounding issue because observations of stratocumulus clouds from Lagrangian experiments over several days do not suggest a strong diurnal cycle in N_d or CCN [e.g., *Bretherton et al.*, 1995; *Johnson et al.*, 2000]. Observations suggest that the diurnal variability in the vertical wind at cloud base is not particularly strong in the MBL [*Hignett*, 1991], and aerosol measurements from the cruises indicate only a modest diurnal cycle in N_a with an amplitude of less than 10% of the mean (not shown). Thus, we would not expect strong differences in cloud droplet concentration between day and night.

[20] Further support that the GOES nighttime BTD contains credible microphysical properties of the MBL over the SEP is presented in Figure 3 which shows a good degree of correlation (r = 0.83 for correlation weighted inversely with sampling errors, r = 0.69 without weighting) between BTD (mean value within 30 km of the ship) for overcast cloudy scenes against the in situ accumulation mode aerosol concentration N_a (averaged over a 1 h period spanning the satellite overpass time) during the 2003 and 2004 cruises. BTD data are taken from both GOES and MODIS nighttime overpasses. Thus, nighttime BTD can explain well over half of the variance in the accumulation mode aerosol concentration in the SEP. This gives us some confidence that variability in BTD is indicative of microphysical variability in stratocumulus clouds.

3.2. MODIS Drizzle Proxy

[21] We introduce a drizzle index derived from Terra MODIS Level 3 daily mean cloud LWP and cloud droplet

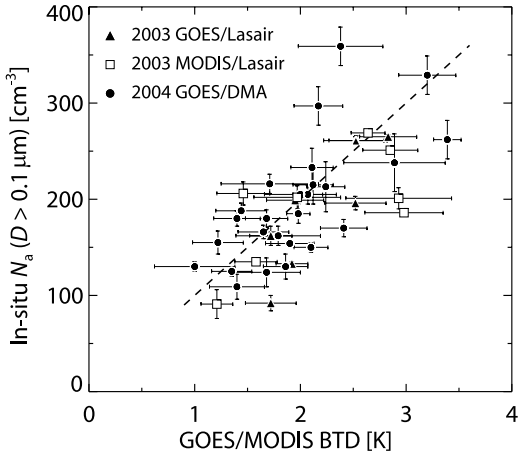

Figure 3. Instantaneous GOES or MODIS BTD means for fully overcast scenes within 30 km of the ship plotted against the in situ accumulation mode aerosol concentration averaged over half an hour centered on the time of the satellite overpass. Error bars indicate sampling errors given at the 2-σ level. The dashed line is a linear fit to the data.

concentration N_d averaged over $1 \times 1°$. The index is first derived for each $1 \times 1°$ box using the diagnostic relationship between cloud base precipitation rate P_{cb}, LWP, and N_d found from surface-based remote sensing [*Comstock et al.*, 2004] in EPIC, namely,

$$P_{cb} = 0.37(LWP/N_d)^{1.75} \quad (1)$$

where P_{cb} is in units of mm d^{-1}, LWP in g m^{-2} and N_d in cm^{-3}.

[22] We average the P_{cb} estimates from the $1 \times 1°$ regions over the region 15–25°S, 80–90°W, i.e., the region of climatological mean maximum low cloud cover for September/October. Because we are wary of retrievals from regions of strongly broken clouds [e.g., *Coakley et al.*, 2005] we only include in the average those $1 \times 1°$ regions that contain >50% low cloud cover. The results presented in this paper are quite insensitive to the precise value of the low cloud cover threshold used. Further, we weight the mean P_{cb} over the cloudy boxes by the cloud cover to further ensure that we are primarily using overcast, and therefore more trustworthy, retrievals. We term this mean quantity the MODIS drizzle proxy (MDP) for the stratocumulus sheet. We discuss the use of the MDP in section 5.1.

3.3. GOES IR Wavelet Variance

[23] We also derive a measure of mesoscale cloud variability which we call the IR wavelet variance. This field is constructed from the field of HH2 wavelet coefficients W_{22} of T_b^{TIR}. At each pixel, W_{22} is a measure of the T_b^{TIR} band-pass-filtered to 8–16 km (2–4 pixel) wavelengths in each of the two horizontal coordinate directions. More precisely, a maximum-overlap discrete wavelet transform based on a LA8 (eighth-order least asymmetric) wavelet filter (see *Cornish et al.* [2006] and *Percival and Walden* [2000] for more details) is applied to each of the rows of the matrix of T_b^{TIR} pixels, which are then overwritten by the resulting level-2 wavelet coefficients to make a new matrix. This effectively band-pass filters T_b^{TIR} in the row-wise direction. The procedure is then repeated on the columns of this new matrix to additionally band-pass filter T_b^{TIR} in the column-wise direction. The advantage of a wavelet transform over a true discrete Fourier band-pass filter is that it is local and thus is less susceptible to bad or missing data and issues with boundary conditions at the edge of the satellite image. The LA8 filter was chosen on the basis of prior experience as a better approximation to a true band-pass filter than the simpler Haar wavelet, though that is probably an unimportant advantage for this application.

[24] The IR wavelet variance at each grid point is then defined as the median of W_{22}^2 over a 100 × 100 km (25 × 25 pixel) box centered at that grid point, after screening out pixels with brightness temperatures less than 273 K, which are assumed to be contaminated with cirrus cloud. The 8–16 km wavelength scale is chosen because it is particularly effective in picking out cloud variations on the length scales seen in POCs, though the level-3 (16–32 km) wavelet coefficients work nearly as well. The 100 km box provides a large enough sample of wavelet coefficients to give a smoothly estimator of cloud variability, yet is small enough to resolve the edges of POCs. Use of a median rather than a mean makes the procedure more robust to pixels with bad data or unscreened high clouds.

4. Case Studies

[25] Two cases studies are presented that provide insight into the formation and growth of regions of open cellular convection in stratocumulus clouds. Both case studies involve observations from satellites and from the 2001 and 2003 cruises (Table 1).

4.1. Case Study of 15–18 October 2001

[26] Figure 4 shows nighttime GOES thermal IR and BTD imagery over a 4 day period (15–18 October 2001) when open cells formed directly from overcast stratocumulus. Note how the open cell regions initially form as small pockets (POCs) within the unbroken clouds, and can be delineated by increasing wavelet variance. The incipient POCs tend to grow as they advect with the mean low-level flow. For example, the relatively small POC that formed over the ship during the early morning hours of 17 October advects approximately 600 km to the WNW of the ship over the subsequent 24 h period, and has grown to cover an area of some 250,000 km^2. Similarly, the POC that formed at 17°S, 81°W on 16 October grows markedly over a 24 h period. Figure 4 also reveals that the open cells form from unbroken cloud with low values of BTD. Tongues of high BTD cloud (such as those centered on 18°S, 82°W on 15 October and 22°S, 78°W on 17 October) tend to remain overcast. POCs, once formed, tend to persist until the cloud field in which they are embedded itself becomes broken.

[27] Isobaric 925 hPa back trajectories are derived each day for two boundary layer air masses using NCEP reanalysis. The first air mass, which we will term the POC-forming air mass, is defined as passing over the ship (20°S, 85°W) at 0845 UTC on 17 October (Figure 4g). The locus of points in this air mass is determined for 15–18 October by isobaric forward and backward trajectories

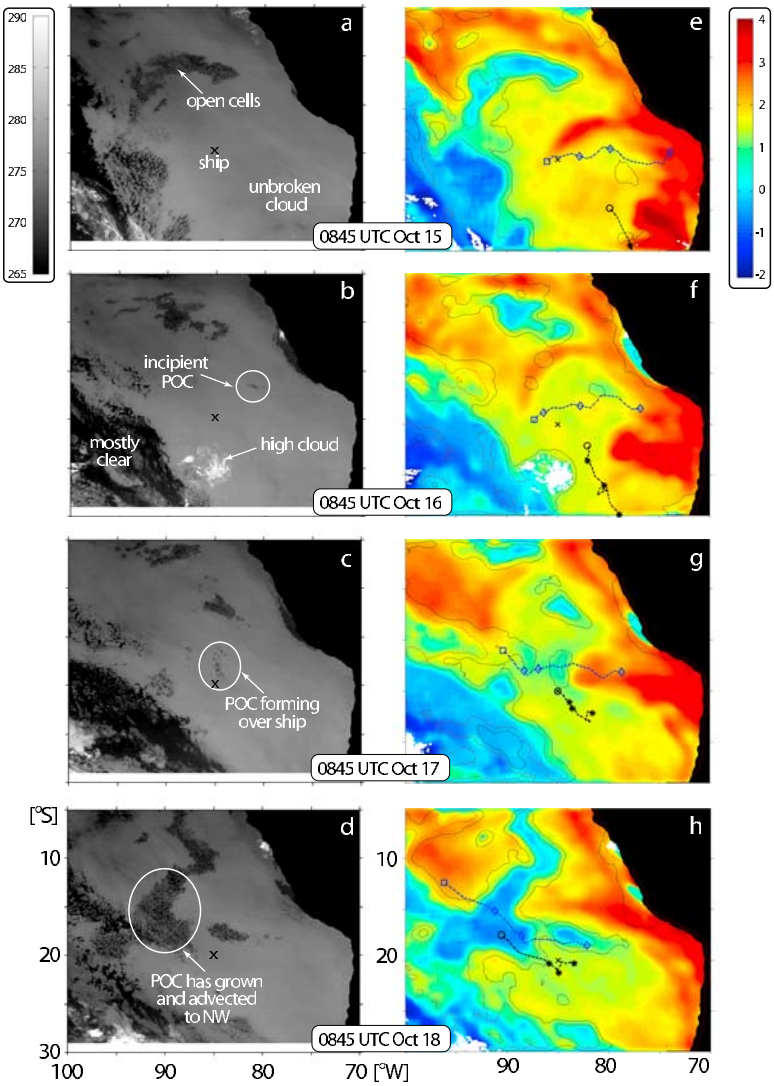

Figure 4. GOES (a–d) T_b^{TIR} and (e–h) BTD for 0845 UTC imagery from four consecutive days (15–18 October 2001). Also shown are contours of T_b^{TIR} HH2 wavelet variance (0.001 red, 0.05 black) in Figures 4e–4h, smoothed using a boxcar median filter over a 25 × 25 pixel box. The ship was situated at 20°S, 85°W throughout (shown by a cross on panels). The black circle and blue square show the locations, estimated using forward and backward 2-D trajectories, of the air masses that passed directly over the ship at 0845 UTC 17 October and 0845 UTC 16 October, respectively. The dashed lines and symbols show 3-D back trajectories for these advected air mass locations with symbols (asterisks or diamonds) plotted every 24 h along the trajectory. The white ellipses on the left show the locations of newly formed POCs, including the one that passes over the ship.

(and is shown as the black circles in Figures 4e–4h). This air mass developed into open cells during the early morning hours as it passed the vicinity of the ship on 17 October (compare Figures 4c and 4d). A second (non-POC-forming) air mass (blue squares in Figures 4e–4h), defined as passing over the ship 2 days before the first (i.e., at 0845 UTC, 15 October, Figure 4e), contained clouds that remained unbroken throughout the period 15–18 October. The non-POC-forming air mass was part of the extended tongue of high BTD centered on 18°S, 82°W at 0845 UTC on 15 October.

[28] At 0845 UTC on each of the 4 days (15–18 October), three-dimensional back trajectories were calculated and are also shown in Figure 4 as the dashed lines marked every 24 h by asterisks for the POC-forming air mass, diamonds for the non-POC-forming air mass. These clearly show marked differences in the origins of the POC-forming and non-POC-forming air masses (or equivalently the regions of low and high BTD). The non-POC-forming air mass originates from the near-coastal region around 20°S,75°W, while the POC-forming air mass originates from the south. This is evidence that the tongues of high BTD, which the analysis in section 3.1 indicates are rich in accumulation mode aerosol, have a continental origin.

[29] Time series from the ship location at 20°S, 85°W (Figure 5) indicate that heavy cloud base drizzle rates (2–3 mm d^{-1}) occurred at approximately the same time as the POC started to form at the end of the night on 17 November (0900–1500 UTC). This association between drizzle and

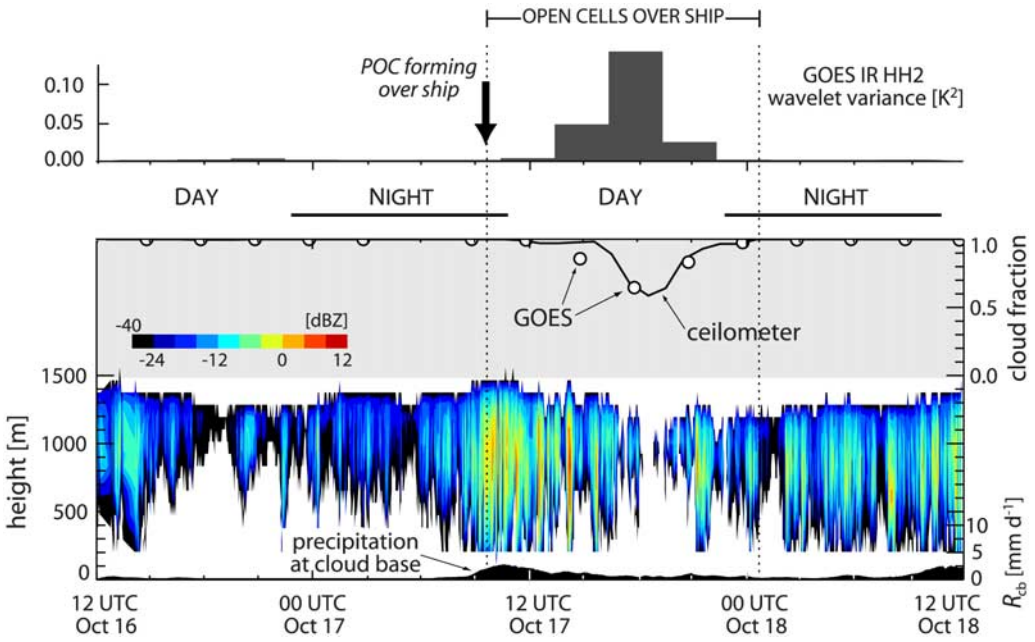

Figure 5. Two day ship time series from 1200 UTC 16 October to 1200 UTC 18 October 2001 detailing changing conditions as a region of open cells forms and moves over the ship at 20°S, 85°W. The panel shows the GOES thermal IR HH2 wavelet variance for a 100 × 100 km box around the ship (top), a time height plot of radar reflectivity from the MMCR (colors), cloud base precipitation rate (filled black), together with cloud cover from the ceilometer (solid line, 3 h means) and from the GOES thermal IR imagery (open circles).

POC formation has previously been noted in observations in the NE and SE Pacific [*Stevens et al.*, 2005; *Sharon et al.*, 2006; *Comstock et al.*, 2007]. Both the satellite and ceilometer cloud fraction drops as the POC grows during the daylight hours of 17 November. Drizzle rates remain substantial (~1 mm d^{-1}) throughout the period where the open cells are over the ship. This period corresponds to high values of the IR wavelet variance.

4.2. Case Study of 14–17 November 2003

[30] The second case study involves the formation and advection of a quasi-linear open cellular feature across the region on 14–17 November 2003. These features are referred to as rifts in the study of *Sharon et al.* [2006]. The images and trajectories in Figure 6 demonstrate that the open cellular feature (marked by the ellipses) is associated with increased wavelet variance. At 0845 UTC on 14 November at around the time when the open cells first formed, the BTD in the overcast clouds is quite low. As the open cell region becomes more defined, the IR wavelet variance increases markedly. For this case, POC and non-POC air masses are defined as passing over the ship at 20°S, 85°W, at 0845 UTC on 16 November and 0245 UTC on 15 November, respectively. In the non-POC air mass, the BTD remains relatively high (BTD >2) throughout the period. There does not appear to be a systematic difference in the origin of the air in the POC and non-POC air masses in contrast to the 2001 case. Neither air mass appears to have passed within 500 km of the coast in the previous 3 days.

[31] Time series at the ship location (Figure 7) reveal that, as with the 2001 case, heavy drizzle is associated with the open cell feature, especially at its leading edge where cloud base drizzle rates are as high at 5–10 mm d^{-1}. Increased IR wavelet variance and reduced cloud fraction accompanies the passage of the open cell region between 0400 and 2400 UTC on 16 November. During the latter half of the feature passage across the ship a substantial reduction in cloud cover occurs between 1500 and 2100 UTC. A 1 km resolution Terra MODIS visible reflectance image at 1550 UTC on 16 November (Figure 8) shows sharp boundaries between the region of open and closed cells and reveals a complex, highly inhomogeneous cloud structure within the open cell region.

[32] Aerosol observations for this case (Figure 7) reveal that accumulation mode aerosol concentrations N_a are as low as 20–40 cm^{-3} in the center of the open cell feature, most likely reflecting the importance of scavenging by precipitation, which can remove CCN at the rate of 30–300 cm^{-3} d^{-1} for precipitation rates found over the SEP [*Wood*, 2006]. Simultaneously, Aitken mode concentrations increased considerably from 100–200 cm^{-3} in the overcast cloud on either side to >500 cm^{-3} in the open cell region itself. Aerosol surface area is very well correlated (r = 0.97), and increases linearly, with N_a [*Tomlinson et al.*, 2007], such that for these data the surface area in μm^2 cm^{-3} is well represented as 0.15 N_a.

[33] During almost the entire period that the open cells were above the ship, the aerosol surface area was lower than 10 μm^2 cm^{-3}. Aerosol models indicate that in the clean MBL, substantial binary nucleation of new particles from sulfuric acid/water can take place when the existing aerosol surface area is lower than approximately 25 μm^2 cm^{-3} [*Raes*, 1995]. Indeed, *Tomlinson et al.* [2007] present evidence of new nucleation for this particular case, and

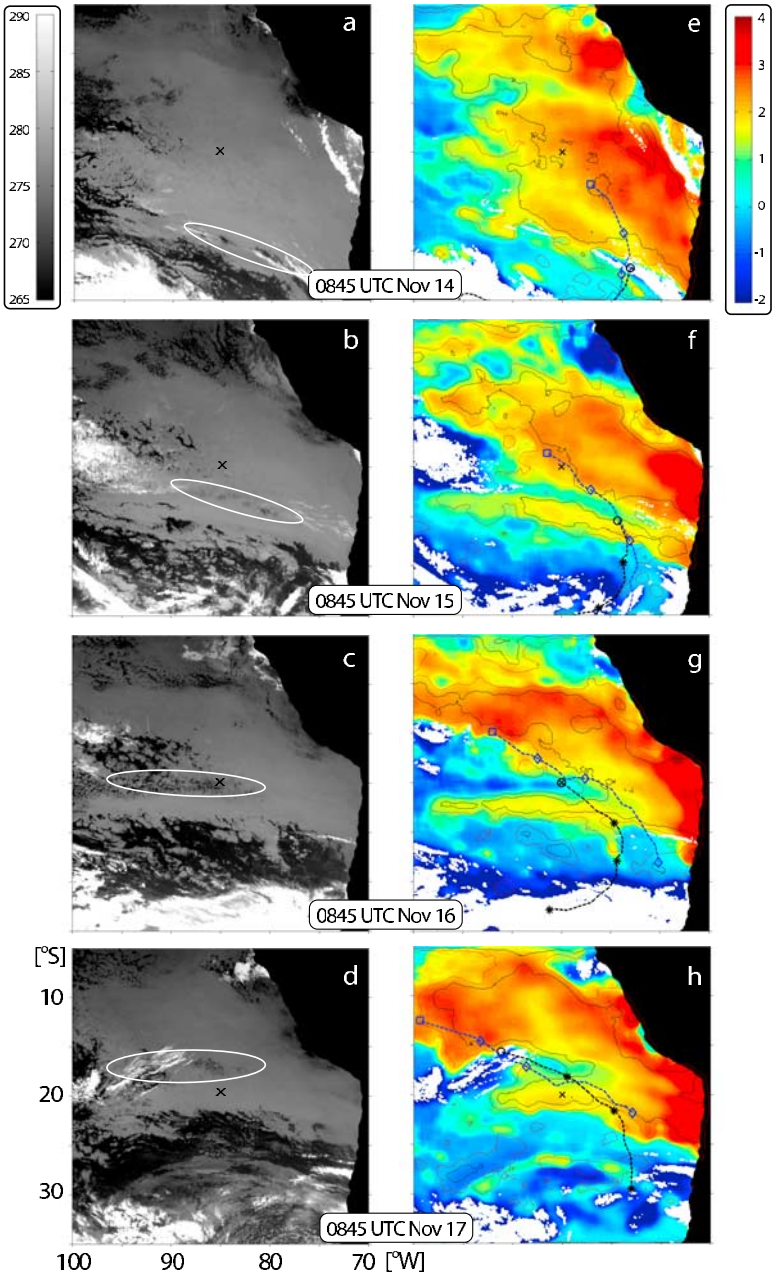

Figure 6. As Figure 4 but for four consecutive days 14–17 November 2003. The white ellipses show the approximate location of the quasi-linear open cellular feature that passed over the ship during 16 October.

demonstrate that this was the most likely cause of the elevated Aitken mode concentrations. Such new nucleation events following precipitation in the MBL have been documented before [*Clarke et al.*, 1998]. The growth of freshly nucleated aerosols to accumulation mode size may be partly responsible for the recovery of aerosol concentrations following drizzle events.

[34] The two case studies illustrate that several characteristics are common to most open cell events over the SEP, e.g., increased heterogeneity, sharply decreased cloud cover, high drizzle rates, and an air mass history that does not appear to be coastally influenced. On the other hand, it does not appear to be possible to determine whether an air mass will contain open or closed MCC on the basis of the back trajectory alone, and the role of low BTD is not completely clear from these studies. In the following sections we take a more statistical approach in our analysis of the characteristics and initiation of open cellular convection.

5. Statistical Analysis

5.1. Frequency of Occurrence

[35] A first attempt at quantitatively assessing the climatology of the MCC type over the SEP using satellites [*Wood and Hartmann*, 2006] reveals strong geographical variability in the frequency of occurrence of open cells, in general

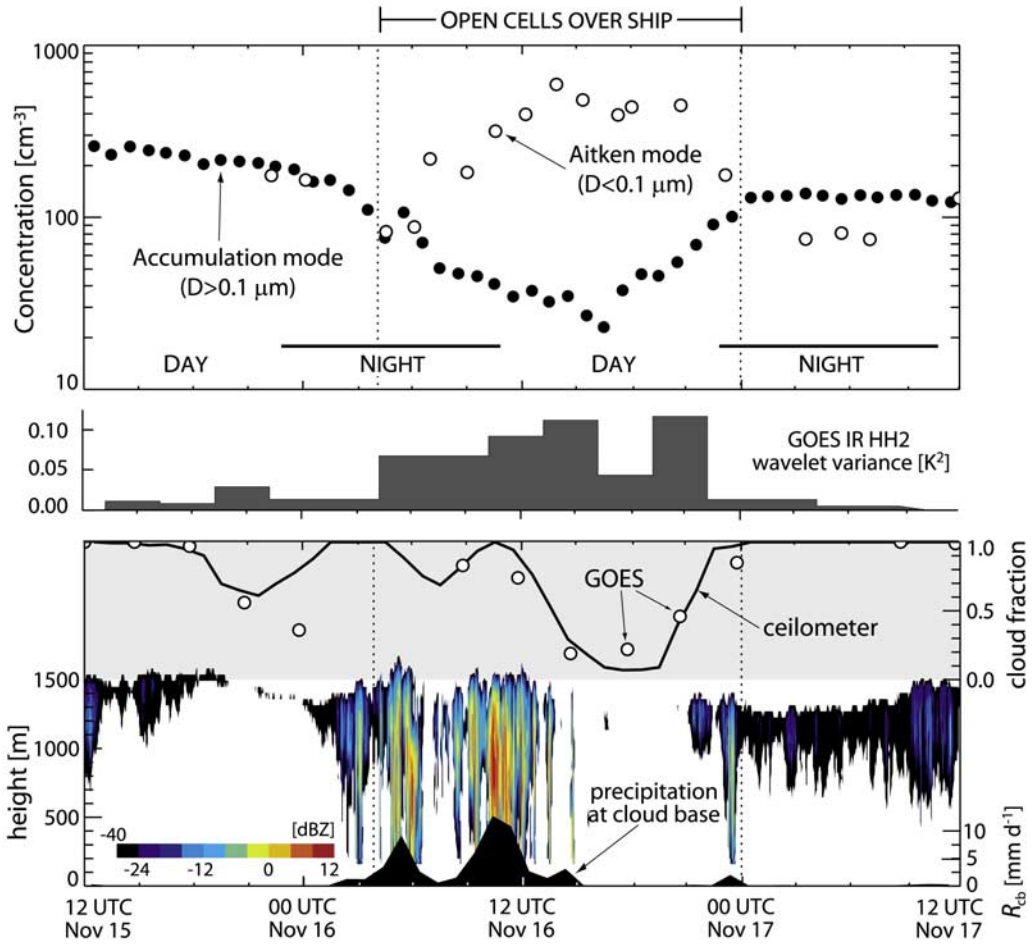

Figure 7. Two day time series from 1200 UTC 15 November to 1200 UTC 17 November 2003 detailing changing conditions as a region of open cells advects over the ship at 20°S, 85°W. (top) Accumulation and Aitken mode aerosol concentrations (closed and open circles, respectively). (middle) The GOES thermal IR HH2 wavelet variance. (bottom) Time-height plot of radar reflectivity from the MMCR (colors), cloud base precipitation rate (filled black), together with cloud cover from the ceilometer (solid line, 3 h means) and from the GOES thermal IR imagery (open circles).

accordance with earlier qualitative assessments [*Agee et al.*, 1973]. *Wood and Hartmann* [2006, Figure 14] found that during September and October 2000 the fraction of 256 × 256 km MODIS scenes classified as open MCC increases from <20% near the South American coast to a maximum of over 50% at 15°S, 100°W. Little is currently known about the temporal variability of the frequency/coverage of open MCC, information that may provide insight into processes controlling the mesoscale structure of low clouds.

[36] Here, we use TIR imagery to examine the temporal variability of the frequency of occurrence of open cells across the region of the SEP dominated by stratocumulus clouds, and to examine the diurnal variability of the formation of pockets of open cells within overcast stratocumulus. Despite attempts to produce an automated routine to classify TIR scenes into different cell types using a wavelet method, we found it impossible to satisfactorily separate regions containing open cells from those containing broken patches of closed MCC such as those at 15°S, 80°W in Figure 8. Because of the strong differences in the optical depth pdf between open and closed cellular regions, visible radiation greatly helps in this separation [*Wood and Hartmann*, 2006]. Thus, we classified GOES TIR images by eye, using as our metric the fraction (discretized into tenths) of the region to the NE of a line joining 30°S, 80°W and 10°S, 100°W that contains open MCC (Figure 9). Throughout this region the seasonal September–October mean low cloud amounts [e.g., *Klein and Hartmann*, 1993] exceed 50%. We will refer to this geographical region as the stratocumulus region. An example of the classification for two scenes, one with an open cell fractional coverage of 50% and the second with <10% is shown in Figure 9b. All the 571 available GOES TIR images (approximately every 3 h) from September/October 2001 were classified in this way.

[37] Figure 9a shows a histogram of the fraction of the region covered by open cellular convection (the open cell fraction, not to be confused with the cloud fraction) in the stratocumulus region. The mean open cell fraction is 0.14 but with a strongly skewed distribution in which open cell fractions of 0.3 or more are present 15% of the time during the time period examined. Accepting that these results are

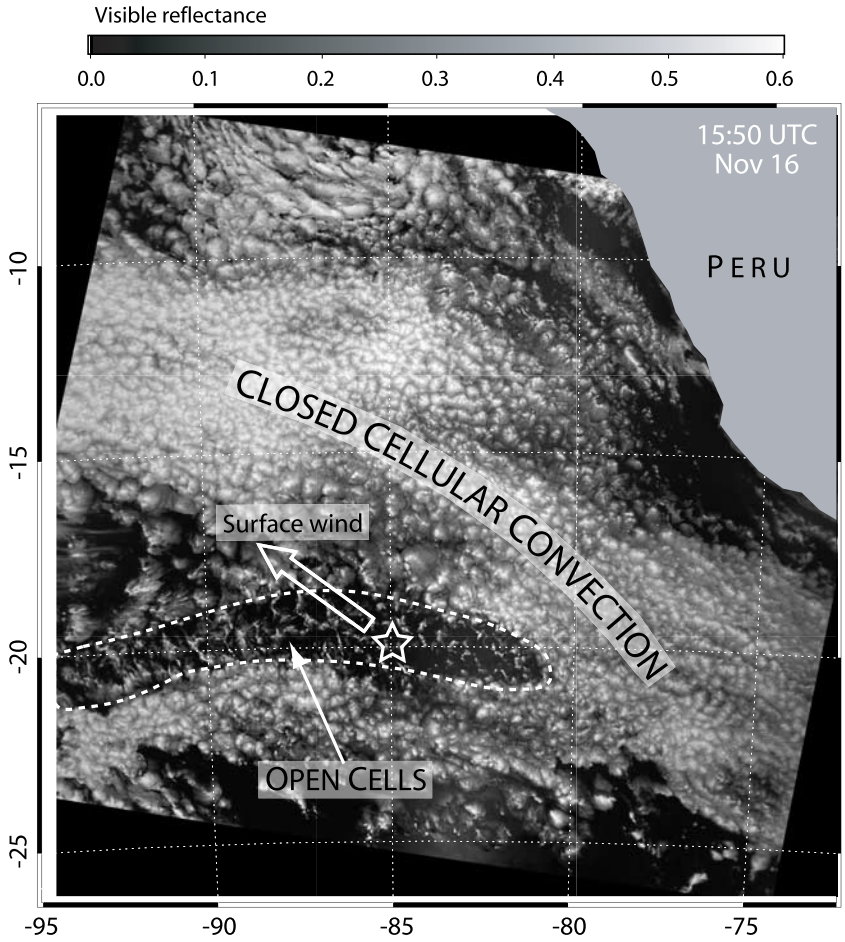

Figure 8. Terra MODIS visible (0.65 μm) reflectance at 1 km resolution from 1550 UTC 16 November 2003 as the region of open cells passes over the ship situated at 20°S, 85°W (star symbol).

somewhat subjective, it is nonetheless instructive to roughly estimate the radiative impacts, which we can do using the regime-dependent (open versus closed cell) mean cloud coverage and liquid water path results from *Wood and Hartmann* [2006]. If all the open cell regions are replaced by closed MCC, then this would result in a mean increase in TOA reflected shortwave radiation of approximately 5 W m^{-2} (or equivalently 5% of the mean) averaged over the entire stratocumulus region. Locally, and at certain times, the impact of open cells can be significantly greater than this.

[38] Figure 9c shows the daily mean open cell fraction over the stratocumulus region for the two month period. Both the magnitude and the long timescale of the variability are striking, with the variability in the daily mean open cell fraction accounting for some 80% of the variance across the entire set of images. Thus there is considerable subseasonal variability in the coverage of the SEP by open MCC, with a decorrelation timescale of approximately 10 days. There are periods (e.g., first week of October 2001) with barely any open cell activity and periods (e.g., the first week of September) where the fractional coverage of open cells exceeds 30%.

[39] The observed subseasonal variability in the prevalence of open cells is interesting and warrants further investigation. The transition from closed to open cells is often associated with strong drizzle formation in the MBL [*Stevens et al.*, 2005; *Sharon et al.*, 2006]. In an attempt to understand the subseasonal variability in open cell fractional coverage, we use the MODIS drizzle proxy (MDP) averaged over the region 15–25°S, 80–90°W as defined in sections 3.2 and 3.3. The MDP is well correlated with the open cell fraction, with $r = 0.69$, significant at the 95% level assuming the series jointly have 10 degrees of freedom (appropriate given the degree of autocorrelation in each series). As a sensitivity test, we carried out the same analysis but with a drizzle proxy that scales with $LWP^{1.5}/N_d$ consistent with the observations by *Van Zanten et al.* [2005] instead of that in equation (1). We found only a small difference in the correlation coefficient between the alternative proxy and the open cell fraction was found to be 0.67 suggesting that the analysis is not highly sensitive to uncertainties in the exact dependency of drizzle upon the LWP and N_d.

[40] The correlation between open cell fraction and MDP is greater than that between open cell fraction and either LWP ($r = 0.40$) or N_d ($r = -0.41$) taken separately. Neither the LWP nor N_d dominates variance in the drizzle proxy. Just 50% of the variance in MDP is explained by variability in LWP alone and only 62% with N_d alone, a conclusion that is also drawn when examining a longer data set (2001–2004).

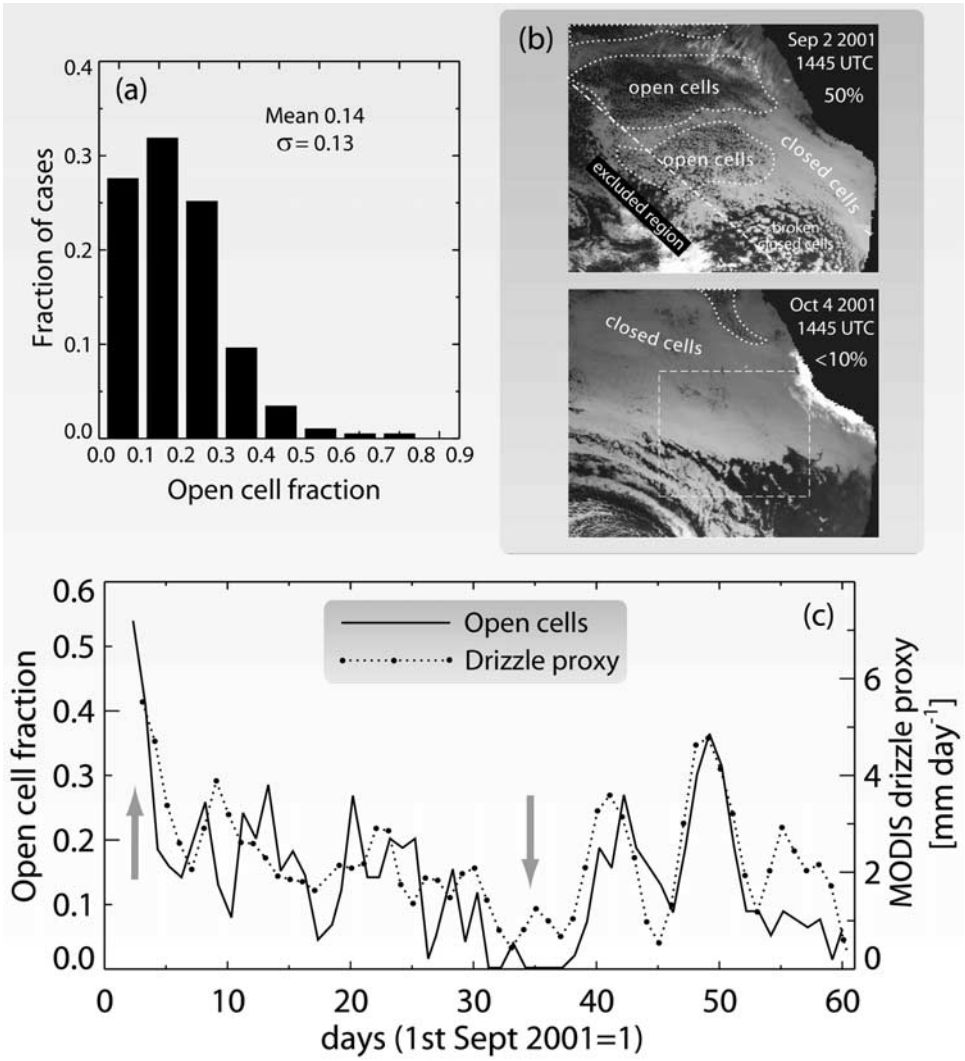

Figure 9. (a) Histogram showing open cell fraction from 571 GOES scenes during September/October 2001; (b) example scenes (5–30°S, 70–100°W) with (top) extensive and (bottom) suppressed open cell activity. The dash-dotted line shows the region excluded from the assessment of open cell fractional coverage (see text). The dashed box shows the region (15–25°S, 80–90°W) over which the MODIS drizzle proxy is averaged. (c) September/October 2001 time series of daily mean open cell fraction (solid line, left axis) and MODIS drizzle proxy (dashed line, right axis).

[41] Our results strongly suggest that both microphysical and macrophysical properties (i.e., LWP) of the stratocumulus clouds are connected to their propensity to support the formation of open MCC. Further, combination of these properties into a variable that evidence shows is strongly related to precipitation [e.g., *Comstock et al.*, 2004] formation results in an improved correlation. This finding constitutes robust additional evidence to support earlier suggestions, based upon a small number of case studies, that the formation of open cells can be linked to precipitation [*Stevens et al.*, 2005].

5.2. Formation

[42] The available GOES TIR imagery from September/October 2001 was used to examine the initial formation of POCs. Visual inspection of sequential images (typically 3 h apart) is used to determine the locations and times at which overcast stratocumulus cloud on one image becomes open cellular clouds on the next image. During the two month period it was possible to identify 23 POC formation events. These data, summarized in Figure 10a, show that approximately two thirds of the POCs form during the early morning hours (0–6 h local). This conclusively demonstrates that POCs do not only form as a result of decoupling of the MBL caused by solar absorption and stabilization during the daytime, and shows that POCs tend to form during periods where there is strong net radiative flux divergence across the MBL. Drizzle tends to peak during the night and early morning hours [*Comstock et al.*, 2004] when the stratocumulus is at its thickest [*Bretherton et al.*, 2004], which lends support to the hypothesis that drizzle is a necessary condition for POCs to form.

[43] Figure 10a also demonstrates that there is a region close to the coast in which POCs tend not to form. Note that this finding does not imply that open cells do not occur close to the coasts, but such features are most commonly of

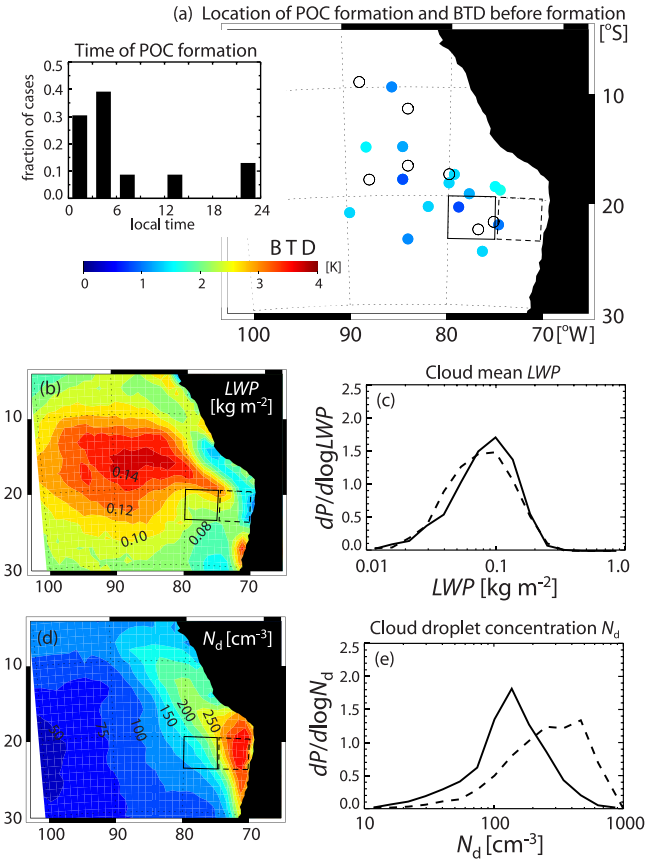

Figure 10. (a) Location and local time (inset) of formation of POCs and the BTD of the cloud prior to POC formation (colors, nighttime formation only). Open circles denote cases where POCs formed in daylight. Boxes show regions that are relatively rich (solid) and relatively devoid (dashed) of POC formation. (b) September/October/November cloud mean (2001–2004) liquid water path from MODIS. (c) PDF of 1° × 1° mean LWP, for POC-prone (solid) and POC-barren (dashed) regions, for all September/October/November MODIS data (2001–2004) with cloud cover >0.8. (d) September/October/November mean MODIS cloud droplet concentration N_d for cloud cover >0.8. (e) PDF of MODIS N_d for POC-forming and POC-barren regions.

the quasi-linear (rift) form (see section 4.2 above) which are advected into the coastal region.

[44] In addition, by examining the nighttime BTD for the GOES image prior to POC formation, an estimate is obtained of the microphysical conditions (i.e., cloud droplet concentration) in the overcast stratocumulus that became the POC. Figure 10a shows that almost universally, these POC-forming stratocumulus exhibited low BTD values, with a mean of 1.4 and minima and maxima of 0.8 and 1.6, respectively. From Figure 2, these values would imply that cloud droplet concentrations less than approximately 100 cm^{-3} are generally required for POCs to form from overcast stratocumulus clouds. Further evidence that POC formation is microphysically limited is presented in Figures 10b–10e which show MODIS-derived mean fields of LWP (for cloudy pixels) and N_d over the SEP, together with pdfs of 1 × 1° means for a region prone to POC formation and a region nearer the coast that is barren of POCs. The mean LWP is higher, and the mean N_d smaller in the POC-forming region. However, there is a much greater fractional difference in N_d than in LWP, and this is clearly shown by the pdfs. If drizzle rates are equally sensitive to fractional changes in LWP and N_d then it would be a reasonable assertion that microphysical variability may play a role in explaining regional differences in POC formation.

[45] Might other factors also influence POC formation? It was suggested by *Stevens et al.* [2005] that a moist free troposphere may be conducive to POC formation as data from some earlier field studies [*Bretherton et al.*, 1995; *Yuter et al.*, 2000; *Stevens et al.*, 2005] have shown a tendency for precipitation to be enhanced when the free troposphere is moist. Figure 11 suggests that a moist free troposphere does not appear to play a major role in the formation of POCs over the SEP. Indeed the data show that when POCs form the free troposphere tends to be drier than normal. One could hypothesize that a moist free troposphere is only one of several possible pathways to precipitation enhancement, and not a way that is particularly favored in the SEP.

6. Meteorological Context

[46] In section 5, we established a correlative link (Figure 9c) between a proxy for drizzle formation (the MDP) and the fraction of the SEP covered by open cellular convection, and found that there is considerable variability in both these parameters on subseasonal timescales. What is the meteorological context associated with this variability, and to what extent is it consistent with previous studies such as *Xu et al.* [2004], which found that regional-scale patterns (i.e., patterns with dominant spatial scales extending over a significant fraction of the SE Pacific subtropical high-pressure region) of meteorological variability can have a strong influence upon liquid water path variability over the SEP?

[47] Here we examine, using composite analysis, the large-scale meteorology associated with low and high

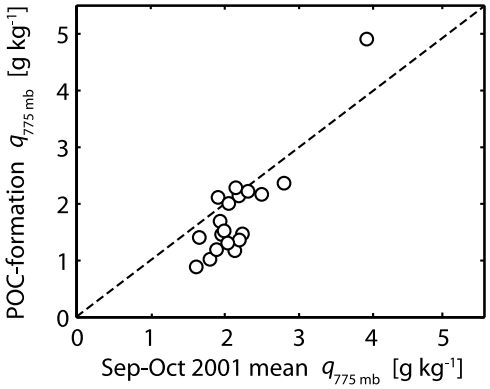

Figure 11. Water vapor mixing ratio at 775 mbar from ERA-40 at the times and locations where POCs formed (Figure 10) against the mean water vapor mixing ratio at each location for September and October 2001. The one-to-one line is also shown.

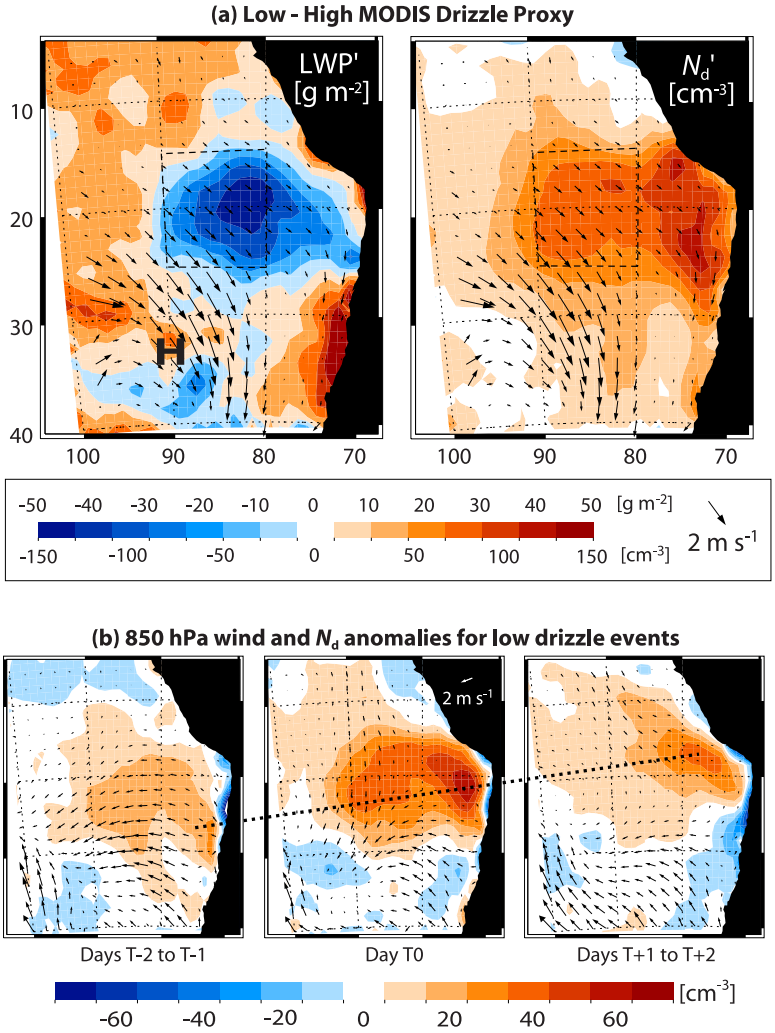

Figure 12. (a) Mean differences in cloud LWP and N_d between days with low MDP minus days with high MDP. Also shown are the equivalent differences in mean surface winds from Quikscat. The mean location of the subtropical high is also shown, together with the region (dashed box) over which the MDP is averaged. (b)Composite evolution of N_d and NCEP 850 hPa wind anomalies over 2 days before the low MDP events, on the day of the low MDP event, and over 2 days after the low MDP event. The dotted line shows that the maximum anomaly in N_d moves northward as the event progresses.

values of the area mean MDP (15–25°S, 80–90°W) using four September/October/November seasons (2001–2004), i.e., a total of 364 days. We choose to examine the differences between low and high values of MDP (rather than the other way around) because the suppression of drizzle, as we shall see, occurs in conjunction with anomalies in N_d that extend along the Chilean coast and may reflect continental pulses of aerosols into the region. If this is indeed the case, then the pertinent issue is one of POC suppression rather than POC formation.

[48] Figure 12a shows maps of the differences in cloud mean LWP and N_d between days with low (MDP <1.25 mm d^{-1}) and high (MDP >2.5 mm d^{-1}) area mean MDP. The low and high MDP days each account for approximately one third of the total days. Not surprisingly, the LWP and N_d anomalies associated with low-high MDP have a large signal in the averaging region, but there are also coherent signals over a larger region, especially for N_d for which the largest signal is to the east of the averaging area. This indicates that the anomalies in MDP are associated with regional-scale variability. The reduced LWP in low MDP periods is associated with somewhat weaker surface winds (the mean surface winds are from the SE within the region of significant negative LWP anomaly). This general pattern is consistent with the major modes of subseasonal variability in LWP seen with the TRMM Microwave Imager (TMI) in the study by *Xu et al.* [2004], who demonstrate that this mode of variability is associated with a weakening anticyclonic circulation (weakening subtropical high) that reduces cold advection, stabilizes the cloud layer, reduces surface moisture flux, and thereby reduces cloud liquid water path.

[49] A new finding is that this mode of regional subseasonal variability is also associated with strong microphysical changes in the stratocumulus, which our results

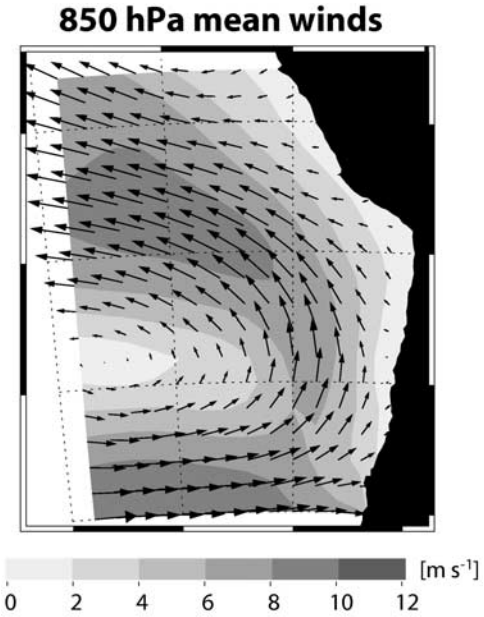

Figure 13. Mean wind field at 850 hPa during September/October/November 2001–2004 from NCEP reanalyis.

suggest are coupled to precipitation variability. To further explore these microphysical patterns, Figure 12b shows the composite evolution of the microphysical changes associated with the low MDP (drizzle suppressed) phase (minus the seasonal mean) over the 5 days centered on the periods of low MDP. Note how the anomaly in N_d appears to move northward along the coast with time, suggesting that the droplet concentration anomalies may be advected with the mean flow. This is consistent with the mean winds (e.g., at 850 hPa as shown in Figure 13) which show near coast-parallel mean flow of a few meters per second (equivalent to ~10 degrees per day).

[50] Little coherent signal is found in the composite surface wind anomaly evolution over this period (not shown), but there is a robust signal in the pattern of 850 hPa winds (Figure 12b, arrows) which distinctly shows offshore flow along the Chilean coast from 20–30°S for the 2 days prior to, and during, the minima in MDP. The 850 hPa winds show zero offshore component in the mean (Figure 13), which makes the mean zonal 850 hPa wind anomaly of -1.5 m s^{-1} in the box 24–34°S, 74–78°W a significant offshore component. This is found despite the necessarily poor representation of the Andean orography in the NCEP model, which smears out the Andes so that the model coastline is to the west of its true counterpart. We hypothesize that these pulses of offshore flow may be responsible for the transport of aerosol-rich continental air from the land west of the Andes over the SEP where it can interact with the marine stratocumulus sheet. The strongest of such offshore transport events have received some prior attention [*Huneeus et al.*, 2006], who found from radiosonde analysis at Antofagasta (23.4°S, 70.4°W) that offshore flow events are frequently associated with mean easterly winds of 5 m s^{-1} or more at 700 hPa. In their study, offshore stratocumulus cloud droplet concentration estimated with MODIS was found to increase significantly during one such easterly wind event, consistent with the simulated pattern of anthropogenic sulfur transport, largely from copper smelting.

7. Discussion

[51] The results presented here demonstrate that strong cloud and aerosol microphysical variability is associated with open cellular convection over the SEP stratocumulus sheet. That the initial formation of POCs tends to occur at night and at times when the cloud droplet concentration in the overcast stratocumulus is low, supports the hypothesis that drizzle plays an important role in the transition from closed to open cells [*Stevens et al.*, 2005], as do recent modeling studies [*Savic-Jovcic and Stevens*, 2008; *Xue et al.*, 2008]. Our finding that low cloud droplet concentrations for overcast stratocumulus observed from space over the SEP are indeed associated with low aerosol concentrations provides some confidence in satellite retrievals of optical depth and effective radius. Implications of our findings are that open cellular convection occurs more frequently when the stratocumulus sheet is prone to drizzle (i.e., when the LWP is high and/or N_d is low), and that a significant fraction of the variability in drizzle over the SEP may be attributable to microphysical, and therefore aerosol, variability. However, it is important to point out that some unknown fraction of the microphysical variability in the MBL is likely to be driven by the large-scale meteorology through effects such as coalescence scavenging of CCN, the rate of which increases strongly with LWP [*Wood*, 2006]. A considerable fraction of the variability in LWP and N_d appears to be associated with patterns of regional meteorological variability, but further work must be carried out to examine the covariation of these critical parameters.

[52] One might be tempted to use our results to suggest that cloud cover over the SEP may have increased since preindustrial times as a direct response to increased anthropogenic activities, the most significant of these being copper smelting which leads to 1.3–1.8 TgS a^{-1} of sulfur emissions, mainly in the forms of sulfur dioxide (SO_2) (source EDGAR3.2 [see *Olivier and Berdowski*, 2001]) from smelters in northern Chile and southern Peru. This SO_2 becomes oxidized to enhance sulfate aerosols. Estimates of natural dimethylsulfide (DMS) emissions over the region of interest are 50–100 mgS m^{-2} a^{-1} [*Boucher et al.*, 2003]. Assuming a relevant emission area of 20 × 30° for DMS would give a total estimate of 0.36–0.72 TgS a^{-1} which is significantly lower than the anthropogenic sulfur sources impacting the SEP. Volcanoes in northern Chile represent an additional natural SO_2 source that is poorly quantified, with only the emissions from a single volcano in northern Chile (Lascar) having been quantified [*Mather et al.*, 2004]. On the basis of a single day of monitoring, the Lascar emissions are estimated to be ~0.5 TgS a^{-1}, but this value must be assumed to be highly uncertain. However, because of their higher elevation (typically 5–6 km and near the continental divide), much of the SO_2 from northern Chilean volcanic emissions may blow eastward across the Andes rather than be swept out over the SEP. It therefore remains a major

challenge to attribute the elevated cloud droplet concentrations we observe over the SEP to specific sources.

8. Conclusions

[53] We have used a combination of satellite, in situ, and reanalysis data sets to study the prevalence, variability, and formation of open cellular convection within the stratocumulus sheet of the SEP. The salient findings are summarized thus:

[54] 1. Case studies of open cellular convection passing over the ship indicate that open cellular convection is associated with increased drizzle, reduced accumulation mode aerosol concentration, and an air mass history that does not pass close to the Chilean coast.

[55] 2. Nighttime values of 11–3.9 μm brightness temperature difference (BTD) for unbroken marine stratocumulus clouds are well correlated with accumulation mode aerosol concentrations measured on a ship below the cloud, suggesting that BTD is a good proxy for cloud droplet concentration in these clouds. This is further supported by the similarity in the pattern of geographical mean BTD and daytime cloud droplet concentration estimated using MODIS visible/near IR retrievals.

[56] 3. The initial formation of pockets of open cells (POCs) occurs most commonly during the later part of the night, and occurs in clouds with low BTD (low cloud droplet concentration). Occurrence was not found to be related to free-tropospheric moisture anomalies.

[57] 4. The frequency of occurrence of open cellular convection over the region of the SEP with extensive climatological low cloud was approximately 10–15% for the period September/October 2001, but exhibited marked subseasonal variability with a characteristic timescale of approximately 10 days.

[58] 5. A satellite drizzle proxy (the MODIS drizzle proxy, or MDP) was defined using the ratio of cloud liquid water path to cloud droplet concentration for predominantly overcast regions of stratocumulus. The MDP was found to be strongly correlated with the frequency of occurrence of open cellular convection, suggesting that open cellular convection tends to form when stratocumulus clouds drizzle.

[59] 6. Composite analysis of the MDP over a longer period suggests that both cloud liquid water path (LWP) and cloud droplet concentration N_d each play major roles in modulating drizzle over the SEP. Minima in MDP are associated with a weakening subtropical high and weaker surface winds which lower the LWP, but also a significant offshore flow prior to the low MDP events which we hypothesize result in pulses of continental aerosol-rich air being transported offshore and into the stratocumulus sheet.

[60] **Acknowledgments.** The stratocumulus cruise of EPIC 2001 was a cooperative effort among many scientists, students, staff, and the crew of the NOAA R/V Ronald H. Brown. The authors gratefully acknowledge support from NSF grants ATM-0082384, ATM-0433712, and DMS-0222115. We gratefully acknowledge NASA GSFC for the provision of MODIS data. GOES data were provided by SSEC, Wisconsin. QuikScat data are produced by Remote Sensing Systems and sponsored by the NASA Ocean Vector Winds Science Team. Data are available at http://www.remss.com. NCEP/NCAR reanalysis data were provided by the Climate Diagnostics Center at NOAA ESRL. ERA-40 data were provided by the European Centre for Medium-Range Weather Forecasts.

References

Agee, E. M., T. S. Chen, and K. E. Dowell (1973), A review of mesoscale cellular convection, *Bull. Am. Meteorol. Soc.*, *54*, 1004–1012.

Bennartz, R. (2007), Global assessment of marine boundary layer cloud droplet number concentration from satellite, *J. Geophys. Res.*, *112*, D02201, doi:10.1029/2006JD007547.

Boucher, O., et al. (2003), DMS atmospheric concentrations and sulphate aerosol indirect radiative forcing: A sensitivity study to the DMS source representation and oxidation, *Atmos. Chem. Phys.*, *3*, 49–65.

Bretherton, C. S., P. Austin, and S. T. Siems (1995), Cloudiness and marine boundary layer dynamics in the ASTEX Lagrangian experiments. Part II: Cloudiness, drizzle, surface fluxes and entrainment, *J. Atmos. Sci.*, *52*, 2724–2735.

Bretherton, C. S., T. Uttal, C. W. Fairall, S. E. Yuter, R. A. Weller, D. Baumgardner, K. Comstock, and R. Wood (2004), The EPIC 2001 stratocumulus study, *Bull. Am. Meteorol. Soc.*, *85*, 967–977.

Clarke, A. D., et al. (1998), Particle nucleation in the tropical boundary layer and its coupling to marine sulfur sources, *Science*, *282*, 89–92.

Coakley, J. A., Jr, M. A. Friedman, and W. R. Tahnk (2005), Retrievals of cloud properties for partly cloudy imager pixels, *J. Atmos. Oceanic Technol.*, *22*, 3–17.

Comstock, K., R. Wood, S. Yuter, and C. S. Bretherton (2004), Radar observations of precipitation in and below stratocumulus clouds, *Q. J. R. Meteorol. Soc.*, *130*, 2891–2918.

Comstock, K., C. S. Bretherton, and S. Yuter (2005), Mesoscale variability and drizzle in southeast Pacific stratocumulus, *J. Atmos. Sci.*, *62*, 3792–3807.

Comstock, K., S. E. Yuter, R. Wood, and C. S. Bretherton (2007), The three dimensional structure and kinematics of drizzling stratocumulus, *Mon. Weather Rev.*, *135*, 3767–3784.

Cornish, C. R., C. S. Bretherton, and D. B. Percival (2006), Wavelet analysis of marine boundary layer turbulence during EPIC, *Boundary Layer Meteorol.*, *119*, 339–374, doi:10.1007/s10546-005-9011-y.

Hignett, P. (1991), Observations of diurnal variation in a cloud-capped marine boundary layer, *J. Atmos. Sci.*, *48*, 1474–1482.

Hoppel, W. A., G. M. Frick, and R. E. Larson (1986), Effect of nonprecipitating clouds on the aerosol size distribution in the marine boundary layer, *Geophys. Res. Lett.*, *13*, 125–128.

Huneeus, N., L. Gallardo, and J. A. Rutllant (2006), Offshore transport episodes of anthropogenic sulfur in northern Chile: Potential impact on the stratocumulus cloud deck, *Geophys. Res. Lett.*, *33*, L19819, doi:10.1029/2006GL026921.

Johnson, D. W., et al. (2000), An overview of the Lagrangian experiments undertaken during the North Atlantic regional Aerosol Characterisation Experiment (ACE-2), *Tellus, Ser. B*, *52*, 290–320.

King, M. D., Y. Kaufman, W. P. Menzel, and D. Tanré (1992), Remote sensing of cloud, aerosol, and water vapor properties from the Moderate Resolution Imaging Spectroradiometer (MODIS), *IEEE Trans. Geosci. Remotr Sens.*, *30*, 2–27.

King, M. D., W. P. Menzel, and Y. Kaufman (2003), Cloud and aerosol properties, precipitable water, and profiles of temperature and water vapor from MODIS, *IEEE Trans. Geosci. Remote Sens.*, *41*, 442–458.

Kistler, R., et al. (2001), The NCEP/NCAR 50-year reanalysis, *Bull. Am. Meteorol. Soc.*, *82*, 247–267.

Klein, S. A., and D. L. Hartmann (1993), The seasonal cycle of low stratiform clouds, *J. Clim.*, *6*, 1588–1606.

Kollias, P., C. W. Fairall, P. Zuidema, J. Tomlinson, and G. A. Wick (2004), Observations of marine stratocumulus in SE Pacific during the PACS 2003 cruise, *Geophys. Res. Lett.*, *31*, L22110, doi:10.1029/2004GL020751.

Mather, T. A., V. I. Tsanev, D. M. Pyle, A. J. S. Gonigle, A. G. Oppenheimer, and C. Allen (2004), Characterization and evolution of tropospheric plumes from Lascar and Villarrica volcanoes, Chile, *J. Geophys. Res.*, *109*, D21303, doi:10.1029/2004JD004934.

Menzel, P., and K. Strabela (1997), Cloud top properties and cloud phase, *Algorithm Theor. Basis Doc., ATBD-MOD-04*, NASA Goddard Space Flight Cent., Greenbelt, Md.

Menzel, W. P., and J. F. W. Purdom (1994), Introducing GOES-I: The first in a new generation of geostationary operational satellites, *Bull. Am. Meteorol. Soc.*, *75*, 757–780.

Olivier, J. G. J., and J. J. M. Berdowski (2001), Global emissions sources and sinks, in *The Climate System*, pp. 33–78, A. A. Balkema, Brookfield, Vt.

Percival, D. B., and A. T. Walden (2000), *Wavelet Methods for Time Series Analysis*, Cambridge Univ. Press, New York.

Pérez, J. C., F. Herrera, F. Rosa, A. González, M. A. Wetzel, R. D. Borys, and D. H. Lowenthal (2000), Retrieval of marine stratus cloud droplet size from NOAA-AVHRR nighttime imagery, *Remote Sens. Environ.*, *73*, 31–45.

Petters, M. D., J. R. Snider, B. Stevens, G. Vali, I. Faloona, and L. M. Russell (2006), Accumulation mode aerosol, pockets of open cells, and particle nucleation in the remote subtropical Pacific marine boundary layer, *J. Geophys. Res.*, *111*, D02206, doi:10.1029/2004JD005694.

Raes, F. (1995), Entrainment of free tropospheric aerosols as a regulating mechanism for cloud condensation nuclei in the remote marine boundary layer, *J. Geophys. Res.*, *100*, 2893–2903.

Rossow, W. B., and W. B. Garder (1993), Cloud detection using satellite measurements of infrared and visible radiances for ISCCP, *J. Clim.*, *6*, 2341–2369.

Savic-Jovcic, V., and B. Stevens (2008), The structure and mesoscale organization of precipitating stratocumulus, *J. Atmos. Sci.*, *65*, 1587–1605.

Sharon, T. M., B. A. Albrecht, H. Jonsson, P. Minnis, M. M. Khaiyer, T. M. VanReken, J. Seinfeld, and R. Flagan (2006), Aerosol and cloud microphysical characteristics of rifts and gradients in maritime stratocumulus clouds, *J. Atmos. Sci.*, *63*, 983–997.

Stevens, B., G. Vali, K. Comstock, R. Wood, M. VanZanten, P. H. Austin, D. H. Bretherton, and C. S. Lenschow (2005), Pockets of open cells (POCs) and drizzle in marine stratocumulus, *Bull. Am. Meteorol. Soc.*, *86*, 51–57.

Szczodrak, M., P. H. Austin, and P. B. Krummel (2001), Variability of optical depth and effective radius in marine stratocumulus clouds, *J. Atmos. Sci.*, *58*, 2912–2926.

Tang, I. N., and H. R. Munkelwitz (1994), Aerosol phase transformation and growth in the atmosphere, *J. Appl. Meteorol.*, *33*, 792–796.

Tomlinson, J. M., R. Li, and D. R. Collins (2007), Physical and chemical properties of the aerosol within the southeastern Pacific marine boundary layer, *J. Geophys. Res.*, *112*, D12211, doi:10.1029/2006JD007771.

Uppala, S. M., et al. (2005), The ERA-40 re-analysis, *Q. J. R. Meteorol. Soc.*, *131*, 2961–3012.

Van Zanten, M. C., and B. Stevens (2005), Observations of the structure of heavily precipitating marine stratocumulus, *J. Atmos. Sci.*, *62*, 4327–4342.

Van Zanten, M. C., B. Stevens, G. Vali, and D. Lenschow (2005), Observations of drizzle in nocturnal marine stratocumulus, *J. Atmos. Sci.*, *62*, 88–106.

Wentz, F. J., and T. Meissner (2000), AMSR Ocean Algorithm, Algorithm Theoretical Basis Document, Technical Report Version 2, Remote Sens. Syst., Santa Rosa, Calif.

Wentz, F. J., and D. K. Smith (1999), A model function for the ocean normalized radar cross section at 14 GHz derived from NSCAT observations, *J. Geophys. Res.*, *104*, 11,499–11,514.

Wood, R. (2006), Rate of loss of cloud droplets by coalescence in warm clouds, *J. Geophys. Res.*, *111*, D21205, doi:10.1029/2006JD007553.

Wood, R., and D. L. Hartmann (2006), Spatial variability of liquid water path in marine boundary layer clouds: The importance of mesoscale cellular convection, *J. Clim.*, *19*, 1748–1764.

Wood, R., P. R. Field, and W. R. Cotton (2002), Autoconversion rate bias in boundary layer cloud parameterizations, *Atmos. Res.*, *65*, 109–128.

Xu, H., S. P. Xie, and Y. Wang (2004), Subseasonal variability of the southeast Pacific stratus cloud deck, *J. Clim.*, *18*, 131–142.

Xue, H., G. Feingold, and B. Stevens (2008), Aerosol effects on clouds, precipitation, and the organization of shallow cumulus convection, *J. Atmos. Sci.*, *65*, 392–406.

Yuter, S. E., Y. L. Serra, and R. A. Houze Jr. (2000), The 1997 Pan American Climate Studies Tropical Eastern Pacific Process Study: part II. Stratocumulus region, *Bull. Am. Meteorol. Soc.*, *81*, 483–490.

C. S. Bretherton, K. K. Comstock, C. Cornish, and R. Wood, Department of Atmospheric Sciences, Box 351640, University of Washington, Seattle, WA 98915, USA. (robwood@atmos.washington.edu)

D. R. Collins, Department of Atmospheric Sciences, Texas A&M University, College Station, TX 77843, USA.

C. Fairall, Earth System Research Laboratory, NOAA, Boulder, CO 80305, USA.

J. Tomlinson, Pacific Northwest National Laboratory, Richland, WA 99352, USA.